Enhancement of flow boiling performance of Zirconium-Silicide ATF by electrophoretic deposition (EPD)

M.R. Kim, H. NOH, T.H. Kim, G.C. LEE
Department of Mechanical Engineering, POSTECH
77 Cheongam-Ro, 37673 Pohang – Republic of Korea

T.K. Kim, H.S. PARK, M.H. KIM
Division of Advanced Nuclear Engineering, POSTECH
77 Cheongam-Ro, 37673 Pohang – Republic of Korea

H. YEOM, H. JO, K. SRIDHARAN
Department of Engineering Physics, University of Wisconsin-Madison
1500 Engineering Drive, WI 53706 Madison – USA

ABSTRACT

Zirconium silicide (ZrSi-Zry) was coated using PVD 3 μm thickness on Zircaloy-4 (Zry-4) for accident tolerance. ZrSi-Zry coated Zry-4 was electrophoretically deposited and characterized. The mean particle size and porosity of the deposit layer were characterized using SEM and FIB analysis. Liquid supplying ability of EPD coated ZrSi-Zry were assessed by liquid rise height measurement. The experiment showed that the wicking performance was higher on EPD coated ZrSi-Zry with the mean particle size of 4.63 μm. Theoretical value of permeability showed that permeability of 4.63 μm case is four times higher than 3.42 μm case. This resulted in higher wicking speed in 4.63 μm case due to the larger pores in structures. As 4.63 μm showed higher liquid rising rate, the flow boiling experiment was performed on the EPD with mean diameter of 4.63 μm. The results on flow boiling experiment showed that Critial heat flux (CHF) was enhanced on EPD coated ZrSi-Zry by more than 50 % compared to ZrSi-Zry at mass flux of 500 kg/m^{2}s. There was a little degradation of boiling heat transfer coefficient (BHTC) on EPD coated ZrSi-Zry in low heat fluxes. However, BHTC of EPD coated ZrSi-Zry became comparable to ZrSi-Zry when heat flux was increased neat the CHF.

1. Introduction

Zirconium-based claddings are vulnerable to oxygen dissolution and hydride precipitation in loss-of-coolant accidents. The loss of the core integrity of Zr-based claddings in loss-of-coolant-accidents had motivated many researchers to develop Accident Tolerant Fuel (ATF) claddings. There are two approaches of ATF cladding, long-term and short-term approaches [1]. The long-term approach refers to the complete change of material from current Zr-alloy to alternative material requiring major modifications of core designs. As a short-term approach, coating of oxidation resistant material on the Zr cladding is readily applicable as the coating does not significantly alter operational characteristics. $ZrSi_2$ possesses self-healing properties and it is easily applicable to the current Zr-alloy due to the material homogeneity [2].

In parallel to the material development, heat transfer enhancement of claddings can contribute to the accident tolerance of claddings as it is related to removing the excessive heat in loss-of-coolant accidents. In previous research, pool boiling performance of ATF coatings has been assessed and enhanced by increasing surface roughness of the coated surface [3]. However, heat transfer performance of Zr cladding with ATF coating has not been assessed.

Heat transfer of the surface can be evaluated by critical heat flux (CHF) and boiling heat transfer coefficient (BHTC). CHF is an attainable heat flux of the surface and it is related to the

safety margin of the cladding in nuclear power plants. BHTC is the heat transfer efficiency of the surface and it can represent heat removal efficiency of the cladding. Enhancement of CHF and BHTC can delay the loss of fuel integrity and more effectively get rid of decay heat in accidental conditions. The heat transfer performance of the cladding should be evaluated in flow boiling as the heat transfer of cladding surfaces occur in the presence of the coolant flow. In flow boiling, the total heat transfer is the summation of nucleate boiling and forced convection heat transfer [4]. As forced convective heat transfer is related to the mass flux, the heat transfer of the surfaces has different performance depending on the mass flux conditions. Forming microstructures on the surfaces can effectively increase boiling heat transfer performance of surface by enhancing wettability and activating more nucleation on the surfaces. CHF is related to the liquid supply rate of the surface and the enhancement of wettability of the surface can increase CHF [5]. The liquid supplying ability of the surface can be optimized by changing the morphologies of the surface and porosity and particle size are the most dominant parameter affecting the capillary wicking performance of the surface [6]. The effects of surface modifications on ATFs have not been assessed in flow boiling due to the early development stage of ATFs.

Electrophoretic deposition is the deposition of the particles in a suspension to the substrate by utilizing the electric field. EPD can produce the surfaces with different morphologies by changing process conditions such as applied voltage or deposition time. In higher applied voltage, the deposition results in the more loosely packed structures and presence of bigger particles on the substrates [7]. Therefore, the porosity and particle size can be optimized by changing the applied voltage. Deposition thickness can be controlled by adjusting the deposition time [8].

In this study, $ZrSi_2$ ATF cladding surface was modified by Electrophoretic Deposition (EPD) to produce porous structures on $ZrSi_2$ PVD coated Zry-4. The two process parameters of EPD, applied voltage and deposition time, were varied to create porous structures with the different morphologies. The SEM images show that bigger particles deposited on surface at applied voltage of 400 V than at 100 V. Wettability of the surfaces were evaluated by wicking experiments to optimize CHF. Wicking performance showed that higher voltage increased wicking speed of the surface due to higher permeability of bigger particles. The flow boiling experiment was performed under two different mass fluxes. The experimental results show that electrophoretically deposited surface enhanced CHF by more than 50 % with less than 10 % degradation of BHTC at low heat flux at mass flux of 500 kg/m^2s compared to the surface without EPD.

2. Surface preparation

2.1 $ZrSi_2$ PVD coating on Zircaloy-4

$ZrSi_2$ coating was deposited on Zircaloy-4(Shenzhen Sunrise Metal Industry Co. Ltd) using PVD. The Zircaloy-4 substrates with the two different dimensions were used for liquid rise height measurement (25 x 40 mm with thickness of 1 mm) and flow boiling experiment (6 x 80 mm with thickness of 1 mm). All Zircaloy-4 substrates were gone through the same polishing (# 220, #1,200 and then to #2,000) and rinsed with acetone, ethanol and water. The $ZrSi_2$ target (American Elements Inc., Los Angeles, CA) with the reported purity higher than 99.5 % was used. The coating thickness of $ZrSi_2$ film was obtained by SEM analysis and it is shown in Fig.1. Contact angle and roughness were measured on Zircaloy-4 (Zry-4) and $ZrSi_2$ coated Zircaloy-4 ($ZrSi_2$) and the data is summarized in Table. 1. PVD increased maximum roughness of the surface by around 50 % due to the formation of bulbous structures as seen in Fig.1. The contact angle was measured with the droplet goniometer (SmartDrop, FemtoFab) with 2 μl water droplet.

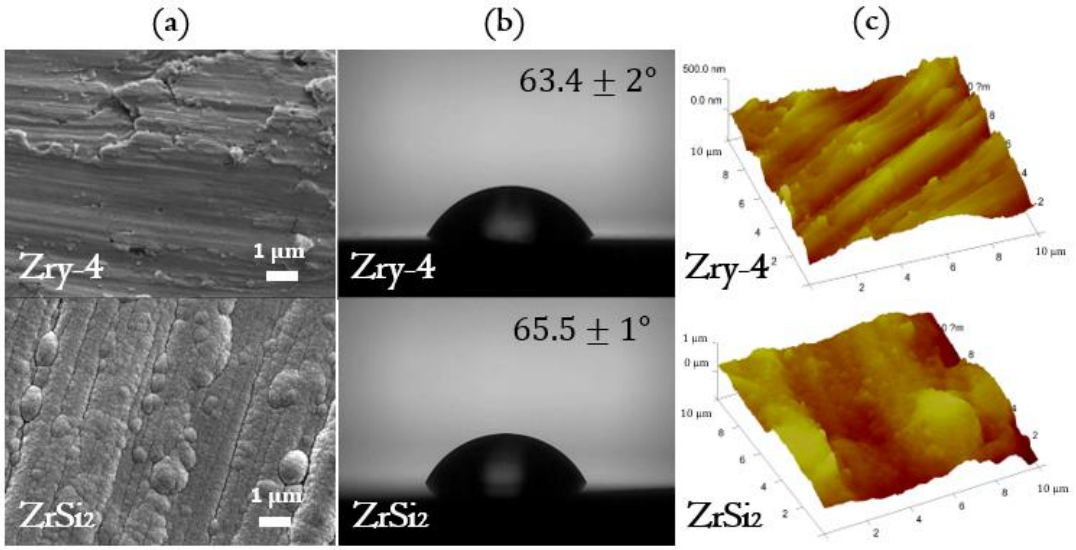

Figure 1. Effect of ZrSi2 PVD coating on the surface characteristics (a) SEM image of Zircaloy-4 (Zry-4) and $ZrSi_2$ PVD coated Zry-4 ($ZrSi_2$), (b) Contact angle measurements on Zry-4 and $ZrSi_2$, (c) AFM roughness measurements on Zry-4 and $ZrSi_2$

Test specimen	Surface roughness	
	R_a (nm)	R_{max} (nm)
Zry-4	**54.8**	**651**
$ZrSi_2$	**116.3**	**898**

Table 1. Average and Maximum roughness on Zry-4 and $ZrSi_2$

2.2 Electrophoretic deposition of $ZrSi_2$ particles on $ZrSi_2$ PVD coated Zircaloy-4

Electrophoretic deposition (EPD) is a deposition of particles in a colloidal suspension to the substrate using an electric field. The schematic of the process is illustrated in Fig. 2 (a). The deposition occurred at the anode and the distance between the anode and counting electrode was maintained to be 2 cm. The $ZrSi_2$ particles with the distribution of Fig. 2 (b) was diluted in Acetylacetone (SigmaAldrich, 99 % purity) and the concentration was maintained to 0.5 % or 1 %. The solution was sonicated for more than 3 hours and deposition was performed in PEEK Jig with 200 ml of solution. The magnetic stirrer aided the dispersion of particles during or prior to the deposition.

Electric field was adjusted to 50 V/cm or 200 V/cm to morphologies of the deposits and the deposition condition is summarized in Table. 2. Higher solid concentration was chosen when the deposition was performed at 50 V/cm as the deposition rate is theoretically 4 times lower than EPDs deposited at 200 V/cm. After the deposition, the deposits were sintered with the heating rate of 100 ℃/hr. When it reaches 500 ℃, the samples were soaked for 1 hour and cooled down with the cooling rate of 100 ℃/hr to the room temperature.

Electric field (V/cm)	Solid concentration (wt%)	Deposition time (s)	Mean particle diameter (μm)	Thickness (μm)	Porosity
50	**1 wt%**	**480**	**3.42**	**4.37±0.64**	**0.53±0.07**
200	**0.5 wt%**	**120**	**4.63**	**5.40±0.49**	**0.64±0.03**

Table 2. Deposition condition for 50 V/cm and 200 V/cm cases

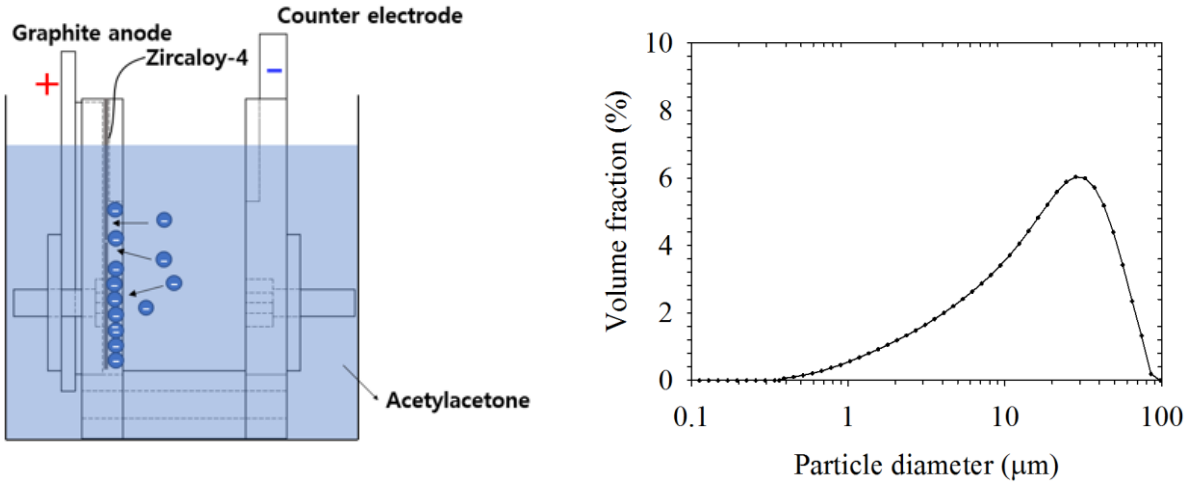

(a) Schematic of electrophoretic deposition (b) Particle size distribution of $ZrSi_2$ particles

Figure 2. Schematic of process and particle size distribution used

2.3 Characterization of Electrophoretic deposition

The particles deposited at different electric fields were collected by sonicating the deposits in a water dispersant. More than four samples were sonicated to dilute $ZrSi_2$ to a water dispersant and particles were then gone through the particle sizer (mastersizer 3000S, Malvern Panalytical). The mean diameter was calculated using the equation below where f_i is the volume fraction at the particle size d_i (μm).

$$d_p = \frac{\sum_{i=1}^{N} f_i d_i}{\sum_{i=1}^{N} f_i} \quad (1)$$

The deposit thickness of the deposits was measured by FIB analysis. FIB was performed by penetrating the three areas with the dimension of 20 μm x 20 μm from the top. The thickness of the samples deposited at the same process condition was measured and the measured thicknesses were averaged by using more than 20 points. The results of FIB analysis are shown in Fig. 5. The average thickness with standard deviations of the samples deposited at 50 V/cm and 200 V/cm were 4.37 ± 0.64 μm and 5.40 ± 0.49 μm respectively.

Based on the thickness of the deposits, the porosity was calculated using the weight of the deposit. The porosity of the deposits was obtained from equation (2). The V_{tot} and $V_{particle}$ refer to the total volume and volume of particles deposited. A and t represent deposition area and mean thickness of the deposit. Due to deviation of the thickness, the uncertainty of porosity is mainly generated by thickness. The characterization results are summarized in Table 2.

$$\varepsilon = \frac{V_{tot} - V_{particle}}{V_{tot}} = \frac{At - W_{particle}/\rho_{particle}}{At} \quad (2)$$

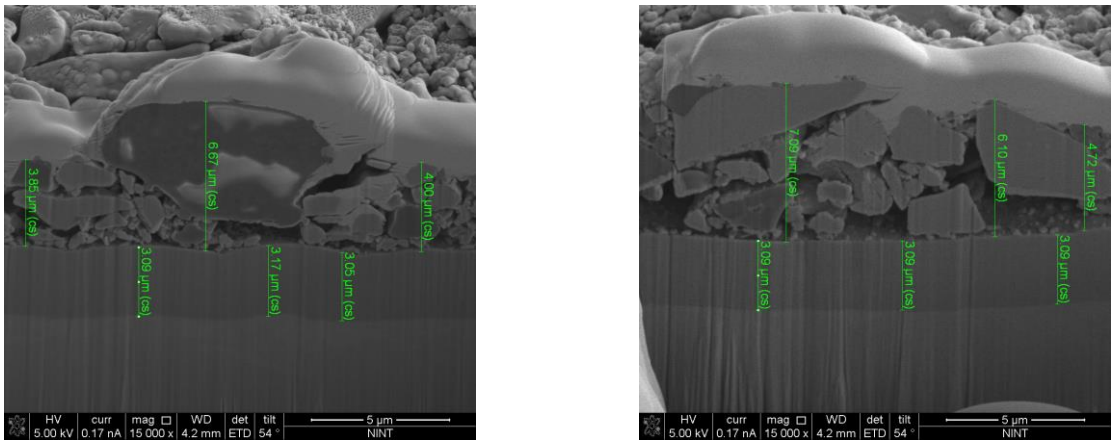

(a) Deposition condition: 50 V/cm (480 s) (b) Deposition condition: 200 V/cm (120 s)

Figure 3. FIB thickness measurements of EPD deposited Zry-$ZrSi_2$

3. Wicking and flow boiling experiments

3.1 Liquid rise height measurement

Liquid rise speed of the deposits was evaluated by the wicking experiment. Liquid inflow rate of the surface is greatly dependent on the liquid supplying ability of the surface and it can be assessed by measuring liquid rise speed. The wicking performance of the deposits was evaluated by measuring liquid rise height of the samples and the detailed explanation on the experiment is described in the previous study [9]. The height of the sample was lowered using clamping tool until it makes the first contact with water. The height of water was recorded by high speed camera (MotionPro Y7, IDT) with 1000 FPS.

3.2 Flow boiling experiment on $ZrSi_2$ and EPD coated on $ZrSi_2$

The flow boiling experiment facility is composed of a primary loop and secondary loop and it is shown in Fig. 4. DI water is used as the working fluid and circulated through the primary loop by a pump. Filter was added and bypassed after the experiment as most particles are spalled after CHF. The working fluid was heated to 96 ℃ passing through the preheater to maintain the inlet fluid temperature. Inside the test section, the fluid direction is vertically upward and condensed to a room temperature by a condenser. The water coming out from the condenser returned to the water tank. The mass flow rate of the fluid was measured with a Coriolis mass flowmeter (RHM06GNT, Reonik). The temperatures and pressures were measured at the inlet and outlet by K-type thermocouples and pressure gauges (280E, Setra for inlet and C206, Setra for outlet).

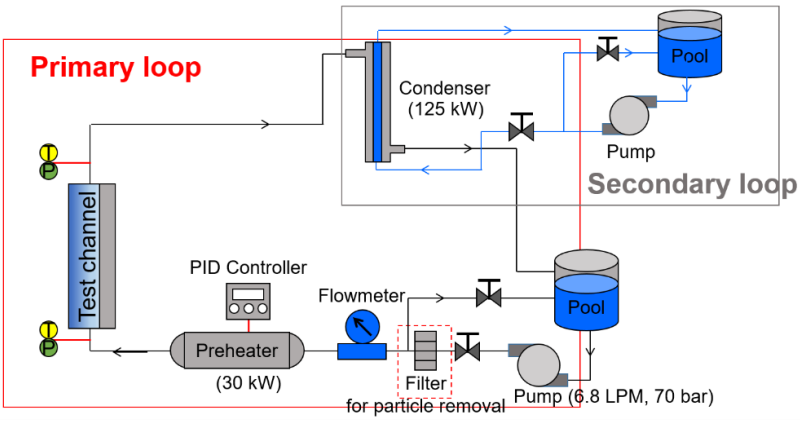

Figure 3. Experimental loop for flow boiling experiment

The test section for the experiment is depicted in Fig. 5. The test channel hydraulic diameter

was determined to be comparable to Westinghouse's 17x17 bundle data [10] which is 8.31 mm. The fluid flows through the acyl window and entrance length more than 40 times of hydraulic diameter was added to fully develop the liquid flow.
The Zry-4 or EPD coated Zry-4 heaters were electrically heated using SCR (60 V, 2500 A) and the heat flux is increased with an increment of 100 kW/m^2 and maintained for 2 minutes at each step. The applied heat flux was calculated by measured voltage and current. The total heat flux was obtained by subtracting the heat loss occurred at wall temperature and the heat loss calculation was based on the previous research [11]. The heat flux and heat flux uncertainties were calculated by the following equations

$$q'' = \frac{VI}{A} - q_{loss}'' \quad (3)$$

$$\frac{U_{q''}}{q''} = \sqrt{\left(\frac{\Delta V}{V}\right)^2 + \left(\frac{\Delta I}{I}\right)^2} \quad (4)$$

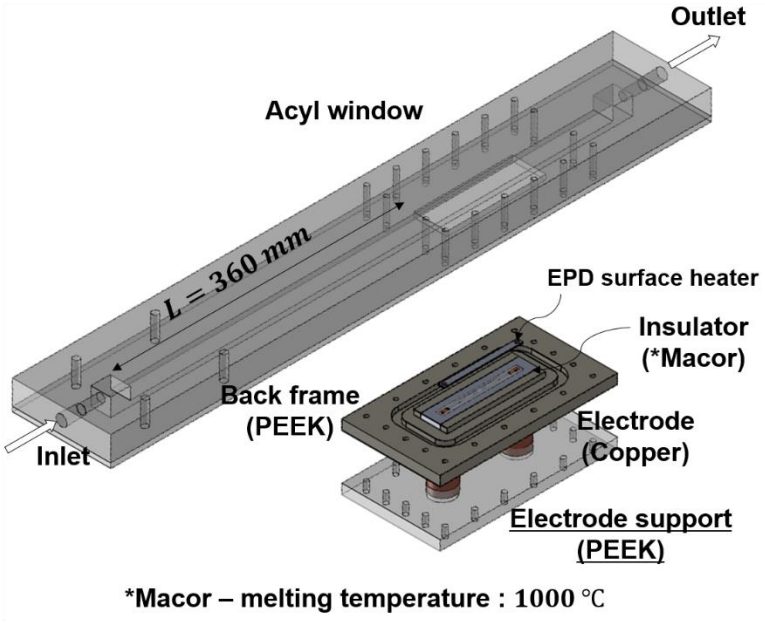

Figure 4. Test section for the flow boiling experiment

The wall temperatures of the heater were estimated using the equations below where T_w represents the measured temperature at the TC, t is the thickness of the heater, x is the location of the TC from the bottom and k is the thermal conductivity of the Zry-4.

$$T_w = T_{TC} - \frac{q''t}{2k} + \frac{q''x^2}{2kt} \quad \cdots (5)$$

$$\frac{dT_w}{dx} = \frac{q''}{kt}x \quad \cdots (6)$$

4. Results and discussion

4.1 Experimental results of liquid rise height measurement

The experimental results of the liquid rise height experiment are plotted in Fig. 6. It shows that liquid rise speed is linear to the time until 0.01 s and became proportional to the square root of the time. The wicking velocities were comparable in both cases and calculated to be 150 mm/s and 146 mm/s. The higher experimental uncertainty existed in 3.42 $\mu\mathrm{m}$ case than in 4.63 $\mu\mathrm{m}$. After 0.01 s, the difference between the two cases became bigger and at 0.05 s, the liquid rise heights in 3.42 $\mu\mathrm{m}$ case and in 4.63 $\mu\mathrm{m}$ case were 3.4 and 3.15 mm.

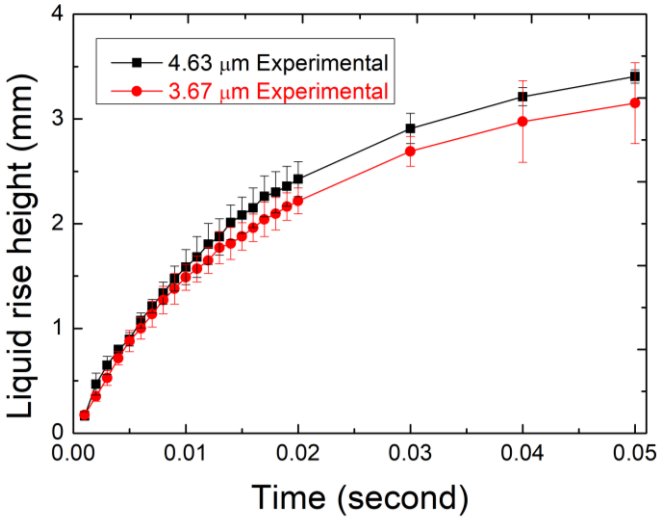

Figure 5. Liquid rise height measurement of the deposit

The liquid rising speed is dependent on the permeability of the porous media according to G. S. Hwang et al., 2010 [9]. The liquid rising rate due to capillary pressure (P_{ca}) can be expressed as the following form.

$$l\frac{dl}{dt} = \frac{K}{\varepsilon\mu}(P_{ca} - \rho g l) \quad (7)$$

where K is permeability, μ is viscosity of the liquid and l is the height of liquid at the given time. The permeability of the deposit can be calculated using the Carman-Kozeny relationship assuming the spherical shape of the particles. The relationship is given by equation (4).

$$K = \frac{\varepsilon^3}{180(1-\varepsilon)^2}{d_p}^2 \quad (8)$$

The permeability for 3.42 μm and 4.63 μm cases was calculated to be 0.0487 and 0.243 μm^2 based on measured ε and d_p. The permeability for 3.6 μm and 4.6 μm cases was calculated to be 0.0487 and 0.243 μm^2 based on measured ε and d_p. As particle shape is highly irregular as seen in Fig. 5, the difference in permeability could explain the higher liquid wicking ability of the 4.63 μm case.

4.2 Experimental results of flow boiling experiment on ZrSi-Zry and EPD ZrSi-Zry (4.63 μm)

The flow boiling experiment was performed on Zry-4, $ZrSi_2$ coated Zry-4 (ZrSi-Zry) and EPD coated ZrSi-Zry (EPD ZrSi-Zry). 4.63 μm case was selected for flow boiling experiment as it showed higher wicking performance compared to 3.42 μm. The flow boiling experiments were performed at mass fluxes of 500 $kg/(m^2s)$ and the pressure on the heater was estimated by assuming linear pressure drop from the inlet to the outlet. The test channel pressures were estimated to be 133 kPa. The boiling curves of Zry-4, ZrSi-Zry and EPD ZrSi-Zry were presented in Fig. 7.

The presence of $ZrSi_2$ PVD coating did not affect the wettability of the surface and it resulted in no change of CHF between Zry-4 and ZrSi-Zry. CHF was enhanced on EPD ZrSi-Zry by 58 % compared to ZrSi-Zry due to capillary inflow in boiling [12]. CHF was greatly enhanced on EPD ZrSi-Zry compared to ZrSi-Zry due to wettability enhancement on porous structures inducing liquid inflow. The ONBs on Zry-4, ZrSi-Zry and EPD ZrSi-Zry were 127.8, 124.5 and 127.5 ℃. The BHTCs were compared at q'' =1400 kW/m^2 on each surface. The BHTCs at this heat flux were calculated to be 40.8, 60.9 and 36.5 kW/m^{2}K. The enhancement of ONB on Zry-$ZrSi_2$

compared to Zry-4 can be explained by the change in roughness of the surface. Due to PVD sputtering, maximum roughness has increased by 38 % on ZrSi-Zry compared to Zry-4. Assuming cavity size is equal to the maximum roughness of the surface, increased maximum roughness might act as active nucleation site enhancing the BHTC [13]. The ONB of ZrSi-Zry was comparable to that of EPD ZrSi-Zry but BHTC decreased on EPD coating especially heat flux lower than 1500 kW/m^2. This can be explained by the relationship between the ONB temperature and contact angle of the surface in pool boiling given by Davis and Anderson [14]. This model relates the contact angle and wettability of the surface and it is represented as equation (9). $q_{w,ONB}{}''$ represents the heat flux occurred at ONBs, σ is the surface tension of the liquid and T_{sat} is the saturation temperature. This model can explain the increase in required wall temperature in super-hydrophilic surface as the coefficient C_1 is the highest in the super-hydrophilic surface.

$$\Delta T_w = \sqrt{\frac{q_{w,ONB}{}'' 8 C_1 \sigma T_{sat}}{k_; h_{fg} \rho_v}}, C_1 = 1 + cos\theta \qquad (9)$$

Therefore, fully developed nucleate boiling (FDB), meaning nucleate boiling on all the heating area, occurred at higher heat flux compared to the surface without EPD resulting in decrease of BHTCs at low heat fluxes compared to ZrSi-Zry. The BHTCs were then improved in higher heat fluxes as nucleate boiling is also fully developed in EPD ZrSi-Zry. BHTC of EPD ZrSi-Zry became comparable to ZrSi-Zry at CHF value of ZrSi-Zry. The BHTCs on Zry-4, EPD ZrSi-Zry were 51.0 and 51.3 kW/m^{2}K at $q'' = 2000$ kW/m^2 (CHF value of ZrSi-Zry) showing no degradation in BHTC.

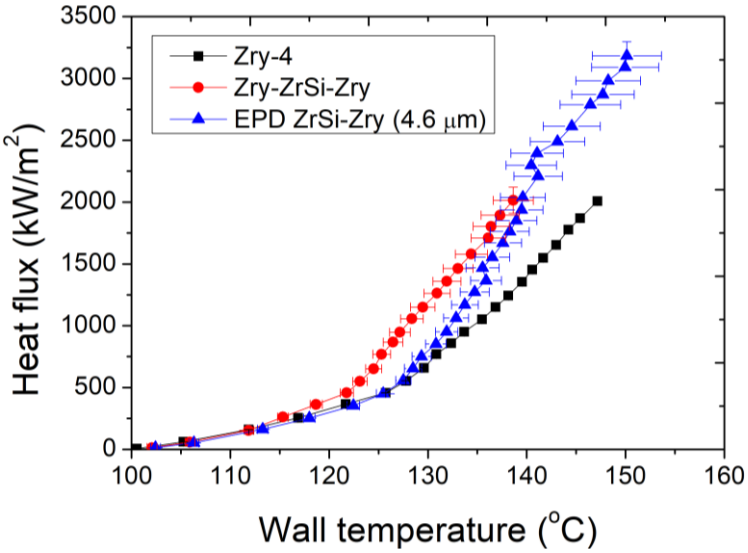

Figure 6. Boiling curves of Zry-4, Zr EPD ZrSi-Zry at G=500 $\mathbf{kg}/\boldsymbol{m^2 s}$

5. Conclusions

$ZrSi_2$ coating was deposited on Zry-4 using PVD and the heat transfer performance of the coating was enhanced with EPD. EPD showed improved liquid inflow rate compared to ZrSi-Zry due to porous structures. The main parameters affecting liquid supply rate of the surface is the particle size and porosity. Prior to flow boiling experiments, the morphologies of the EPD coated ZrSi-Zry were characterized to measure porosity and particle size of the deposits. Liquid supplying ability of 3.42 $\mu\mathrm{m}$ and 4.63 $\mu\mathrm{m}$ were evaluated by liquid rise height measurement experiment and it showed that liquid rising speed on 4.63 $\mu\mathrm{m}$ was higher than on 3.42 $\mu\mathrm{m}$ case due to enhanced liquid permeability.

The flow boiling experiments were performed on bare Zry-4, ZrSi-Zry and EPD ZrSi-Zry at mass flux of 500 kg/(m^2s). The heat transfer was assessed in terms of CHF, ONB and BHTC. The $ZrSi_2$ PVD coating increased the surface roughness resulting in enhanced BHTC compared to Zry-4. CHF value was maintained as both surfaces showed comparable wettability. EPD coating of 4.63 μm was applied on ZrSi-Zry and it showed that CHF and BHTC were all improved compared to Zry-4 and CHF value was improved by 58 %. However, BHTC was decreased at low heat fluxes compared to ZrSi-Zry as transition to FDB occurs at higher heat flux on super-hydrophilic surfaces. The BHTC of EPD ZrSi-Zry began to increase at heat flux higher than 1500 kW/m^2 and it became comparable to ZrSi-Zry at its CHF value (2000 kW/m^2).

Acknowledgement
This research was supported by the National Research Foundation of South Korea (NRF) grant from the Korean government (NRF-2015M2A8A2074795).

6. References
[1] Kang, Y. J., Kim, T. K., Lee, C. L., Kim, M. H., Park, H. S. (2018). Quenching of candidate materials for accident tolerant fuel-cladding in LWRs. Annals of Nuclear Energy, 112, 794-807.
[2] Yeom, H., Maier, B., Mariani, R., Bai, D. and Sridharan, K. (2016). Evolution of multilayered scale structures during high temperature oxidation of $ZrSi_2$. Journal of Materials Research, 31, 3409-3419.
[3] Seo, G. H., Jeun, G., Kim, S. J. (2016). Enhanced pool boiling critical heat flux with a FeCrAl layer fabricated by DC sputtering. International Journal of Heat and Mass Transfer, 102, 1293-1307.
[4] Chen, J. C. (1966). Correlation for boiling heat transfer to saturated fluids in convective flow. Industrial & Engineering Chemistry Process Design and Development, 5 (3), 322-329.
[5] Kim, M. H. and Kim, H. D. (2007). Effect of nanoparticle deposition on capillary wicking that influences the critical heat flux in nanofluids. Applied Physics Letters, 91, 014104.
[6] Wang, D., Wang, X., Zhou, P., Wu, Z., Duan, B. and Wang, C. (2014). Influence of packing density on performance of porous wick for LHP. Powder Technology, 258, 6-10.
[7] I., Z. and L., G. (1997). Electrophoretic deposition of hydroxyapatite. Journal of Materials Science: Materials in Medicine, 8, 213-219.
[8] Chena, C.-Y., Chena, S.-Y. and Liub, D.-M. (1999). Electrophoretic deposition forming of porous alumina membranes. Acta Materialia, 47, 2717-2726.
[9] Hwang, G. S., Nam, Y., Fleming, E., Dussinger, P., Ju, Y. S. and Kaviany, M. (2010). Multi-artery heat pipe spreader: Experiment, 53, 2662-2669.
[10] O' Donnell, G. M., Scott, H. H. and Meyer, R. O. (2001). A new comparative analysis of LWR fuel designs.
[11] Harirchian, T. and Garimella, S. (2008). Microchannel size effects on local flow boiling heat transfer to a dielectric fluid, 51, 3724-3735.
[12] Ahn, H. S., Jo, H. J. and Kim, M. H. (2011). Effect of liquid spreading due to nano/microstructures on the critical heat flux during pool boiling, 98, 071908.
[13] Hsu, Y. Y. (1962). On the Size Range of Active Nucleation Cavities on a Heating Surface, 84(3), 207-213.
[14] Davis, E. J., Anderson, G. H. (1966). The Incipience of Nucleate Boiling in lo1 Forced Convection Flow, AIChE Journal, 12, 774-780.